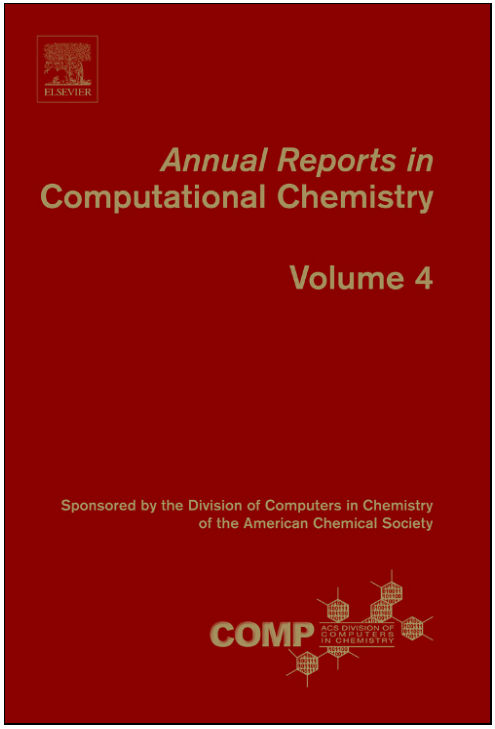

From Huan-Xiang Zhou, Sanbo Qin and Harianto Tjong, Modeling Protein–Protein and Protein–Nucleic Acid Interactions: Structure, Thermodynamics, and Kinetics. In: Ralph A. Wheeler and David C. Spellmeyer, editors, Annual Reports in Computational Chemistry, Volume 4. Amsterdam: Elsevier, 2008, p. 67
ISBN: 978-0-444-53250-3

Elsevier

CHAPTER 4

Modeling Protein–Protein and Protein–Nucleic Acid Interactions: Structure, Thermodynamics, and Kinetics

Huan-Xiang Zhou[*,1], **Sanbo Qin**[*], and **Harianto Tjong**[*]

Contents

1. INTRODUCTION

It is now increasingly recognized that proteins function in the context of multi-component complexes. This review aims to cover recent progress in modeling fundamental properties of proteins in their interactions among themselves and

* Department of Physics and Institute of Molecular Biophysics, Florida State University, Tallahassee, Florida 32306, USA
hzhou4@fsu.edu (H.-X. Zhou)
[1] Corresponding author.

Annual Reports in Computational Chemistry, Vol. 4
ISSN 1574-1400, DOI: 10.1016/S1574-1400(08)00004-2

with nucleic acids. We pay special attention to computational papers which appeared in the past three years, but experimental papers and earlier computational papers which we find particularly relevant are also discussed.

We focus on four interrelated aspects of protein–protein and protein–nucleic acid interactions. Section 2 deals with building structural models for protein complexes. In Section 3 we present an overview of the various methods for computing contributions to the stability of protein complexes. In Section 4 the focus shifts to the rates of forming protein complexes. Finally in Section 5 we discuss the impacts of protein dynamics on the structures, thermodynamics, and kinetics of protein complexes.

2. BUILDING STRUCTURAL MODELS

As a result of favorable interactions, a protein and its partner(s) will form a stereospecific complex. Under favorable conditions, the structure of this complex can be determined by X-ray crystallography, NMR, or electron microscopy. The structure holds the key to understanding the interactions involved and is the basis for making computations on the stability and rate of complex formation.

In many cases, for practical or technical reasons (as opposed to any fundamental physical reasons), the structures of protein complexes cannot be determined experimentally. If the structure of a protein complex with adequate sequence similarity is available, one can build the structure of a query complex by homology modeling [1–3]. The applicability of homology modeling to protein complexes is still limited because the current structural database provides only a sparse coverage of the protein interaction space.

The general approach which aims to build the structure of a complex, starting from the structures of the unbound partners, is now referred to as docking. A forum that provides a fair and critical assessment of various docking methods is the CAPRI "experiment" (http://www.ebi.ac.uk/msd-srv/capri/) run by Joël Janin. We strongly urge method developers to participate in CAPRI, and at the minimum, use the CAPRI targets as a test set. Interested readers can find the latest progress report on CAPRI in a special issue of Proteins (Vol. 69, Issue 4, December 2007).

In general, docking methods aim to maximize the shape and/or physiochemical complementarity between binding partners through generation of large sets of possible poses. Both the sampling of relevant poses and the discrimination of near native poses from the large number of non-native alternatives present significant challenges. The task becomes even more daunting when complex formation is accompanied by rearrangement of loops or relative movement of domains. In our (admittedly biased) opinion, a fruitful approach is to make use of any experimental information available on the interaction [4–7]. Interaction sites can also be predicted by various bioinformatics approaches (for a recent review, see [8]), and from a set of known interfaces by screening [9,10].

We briefly mention two related subjects. For obvious reasons, the interfaces of protein complexes have been a target for developing drug molecules. This subject

has been reviewed in this series [11]. In addition, it has now become possible to design de novo complexes, either by modifying a monomeric protein into a dimeric form [12] or by grafting from an unrelated protein complex [13].

3. PREDICTION OF BINDING AFFINITIES

The stability of protein complexes is measured by the binding constant (K_a). Experimentally determined values of K_a span over 10 orders of magnitude (see Figure 4.1). It is clear that no simple correlations exist between structures of protein complexes and their binding affinities. General approaches to calculating binding affinities have been reviewed [14]. Here we focus on aspects specific to protein–protein and protein–nucleic acid complexes.

The binding constant is given by [14,15]:

$$K_a = \int_{\Gamma} d\mathbf{r}\, d\omega\, e^{-W(\mathbf{r},\omega)/k_B T} \tag{1}$$

where $W(\mathbf{r}, \omega)$ is the potential of mean force of for the interaction between a protein and its partner at a relative separation $\mathbf{r}$ and relative orientation ω, $k_B T$ is thermal energy, and Γ denotes the region of configurational space defining the bound state. Contributing factors to $W(\mathbf{r}, \omega)$ include hydrophobic and electrostatic interactions, and the change in conformational entropy of the binding partners upon complex formation. Typically, computations aim to predict the change in the binding free energy, $-k_B T \ln K_a$, e.g., due to a point mutation.

3.1 Electrostatic contribution

It is well understood that hydrophobic interactions make favorable contributions to binding. However, the effects of electrostatic interactions are subtle. Neglecting conformational changes, the electrostatic contribution is given by

$$W_{el} = G_{el}(AB) - G_{el}(A) - G_{el}(B) \tag{2}$$

where G_{el} is the electrostatic free energy of each subunit (A or B) or the complex (AB), which can be calculated by solving the Poisson–Boltzmann (PB) equation. The subtlety of the electrostatic contribution can be appreciated by decomposing it into two components: the desolvation cost W_{desol} and the solvent-screened interaction energy W_{int} (Figure 4.2). To obtain W_{desol}, the electrostatic solvation energy of each subunit is calculated twice, first by itself and then in the presence of its partner, which has its partial charges zeroed out. The difference in the results between these two calculations gives the desolvation cost for that subunit, and adding the corresponding quantity for its partner gives W_{desol}. The difference between W_{el} and W_{desol} comes from the interactions between the partial charges of the two subunits in the solvent environment.

It is clear that W_{desol} opposes binding. W_{int} will favor binding when the charges on the two subunits have complementary charge distributions, which should be

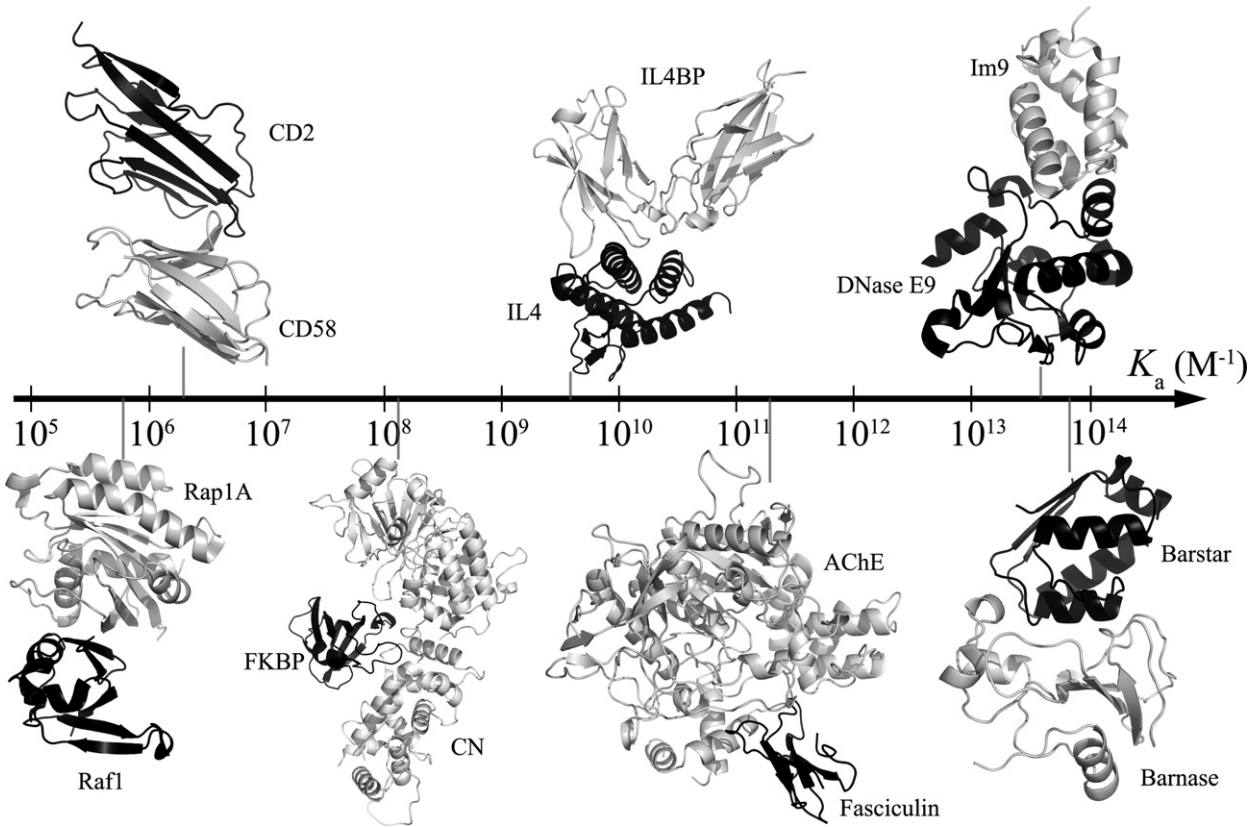

FIGURE 4.1 The spectrum of protein affinities. The locations of seven protein–protein complexes within the spectrum, along with their structures, are shown. Adapted from Dong and Zhou [17].

FIGURE 4.2 Decomposition of the electrostatic contribution to binding affinity into desolvation cost and solvent-screened interaction. Interactions of protein charges with the solvent (represented by shadows around binding molecules) are indicated by outgoing arrows. Upon binding, the binding molecules are desolvated within their interface and charge–charge interactions, as indicated by a double-headed arrow, emerge.

true in general. There W_{el} consists of two opposite components. Whether electrostatic interactions make a net positive or net negative contribution to binding rests on the balance between the two components. In particular, the balance is very sensitive to how the boundary between the protein low dielectric and the solvent high dielectric is precisely specified. As shown on a large number of protein–protein and protein–RNA complexes [16–19], when the dielectric boundary is chosen as the molecular surface (MS), as is often done in the literature, W_{desol} outweighs W_{int}, leading to net destabilization. However, when the dielectric boundary is switched to the van der Waals (vdW) surface, the situation is reversed and electrostatic stabilization is now predicted.

How can one then decide on the choice of the dielectric boundary? One possibility is to benchmark PB calculations against explicit-solvent molecular dynamics (MD) simulations. Most of such efforts have been limited to small solute molecules [20–22]. However, it has been shown that the difference between MS and vdW results for electrostatic solvation energies depends on solute size [23]. Therefore parameterization on small solutes (either against explicit-solvent MD results or against experimental data) may not be reliable for calculating electrostatic contributions to protein–protein and protein–nucleic acid binding.

One can benchmark PB calculations directly against experimental data on protein–protein and protein–nucleic acid binding affinities. Potentially one type of useful data is the dependence of binding affinities on salt concentration. The screening of electrostatic interactions by salts can be captured by the PB equation (it should be mentioned that salts can also specifically bind to proteins and nucleic acids; such specific salt effects require special treatment). Unfortunately, it has been found that the screening effects predicted by MS and vdW calculations are essentially identical and thus cannot discriminate between the two choices of the dielectric boundary [16,18]. On the other hand, effects of mutations involving charged or polar residues have been found to have discriminating power, with experimental data favoring the vdW surface as the choice for the dielectric boundary [16–18]. Experimental data for mutational effects on binding affinity continue to accumulate in the literature [24,25], providing opportunities for comprehensive benchmarking of PB calculation protocols.

In the literature, the MS is still widely chosen as the dielectric boundary. The difference between this choice and the vdW surface is that, according to the latter protocol, the many crevices in the protein interior are treated as part of the solvent high dielectric. These crevices are not accessible to a spherical solvent used in defining the MS, and hence their being treated as part of the solvent dielectric is perceived as unrealistic or undesirable. However, this perception is open to question. Water molecules can access protein interiors, as demonstrated by many protein X-ray structures with water occupying interior positions, by the observation of positionally disordered water molecules in a hydrophobic cavity of interleukin 1β [26] (Figure 4.3), and by molecular dynamics simulations [27]. In proteins like myoglobin and acetylcholinesterase (featuring a deeply buried active site connected to the exterior only through a narrow gorge), access by small molecules like water, made possible by the dynamics of the proteins, is essential for biological functions. We suggest that the vdW protocol provides a way to ac-

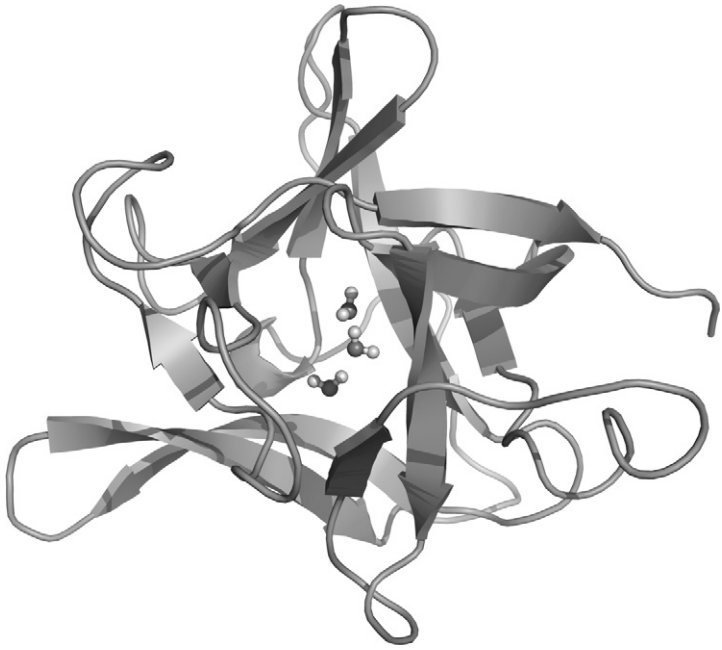

FIGURE 4.3 The presence of water molecules inside a hydrophobic cavity of interleukin 1β. The cavity is separated from the bulk solution according to the MS criterion but connected to the bulk solution according to the vdW criterion. When the three water molecules are moved from separate positions in the bulk solution to the configurations shown inside the cavity, the MS protocol predicts an increase of 0.9 kcal/mol in electrostatic free energy whereas the vdW protocol predicts a decrease of -2.2 kcal/mol.

count for water access to protein interiors. Failure to account for this important property is perhaps the cause for overprediction of pK_a shifts by the MS protocol (which is often "corrected" by increasing the protein dielectric constant to 20). In principle the vdW protocol can be mimicked by the MS protocol with appropriately reduced atomic radii. However, it has been found the precise amount of radius reduction varies from protein to protein and thus mimicking one protocol by the other appears to be a futile exercise [23]. We will come back to the debate between MS and vdW in Section 4.3.

The generalized Born (GB) model has been developed as a fast substitute of the PB equation [28–31]. The GB model can be tailored to match PB results for electrostatic solvation energies obtained by either the MS or the vdW protocol. The errors of GB results in reproducing the PB counterparts are at least of the order of typical mutational effects on binding affinities. Therefore caution should be exercised when applying the GB model to calculate mutational effects.

There is also progress in the opposite direction, i.e., toward more accurate modeling of electrostatic effects, by accounting for electronic polarization via quantum mechanical treatments [32,33]. Such treatments have not been used to directly predict the effects of mutations on the binding free energy, but it is already clear

that electronic polarization can significantly influence electrostatic contributions to binding.

Comparing PB or GB calculations against experimental data for mutational effects on binding affinity is premised on the assumption that the mutational effects are assumed to be dominated by electrostatic contributions. That is, possible contributions by hydrophobic interactions and by changes of conformational entropy are not taken into consideration.

3.2 Other contributions

The limitations listed in the last paragraph are dealt with by the molecular mechanics Poisson–Boltzmann surface area (MM-PBSA) method [34,35]. Like before, the electrostatic contribution is calculated by solving the PB equation, but now the hydrophobic contribution is also calculated (as a linear function of the buried surface area), as is the change in conformational entropy [from (quasi)harmonic analyses of conformational fluctuations]. (There is also a version in which PB is replaced by GB [36].) In recent applications, this method has been used to validate homology models of protein–protein complexes [37] and to elucidate molecular bases of promiscuity and selectivity of protein–protein binding [38,39]. Extensions include using different protein dielectric constants for different types of mutated residues [40] and a simplified way of calculating the change in conformational entropy [41].

Another approach, called linear interaction energy (LIE) [42], is somewhat similar to the MM-PBSA method. Here the electrostatic and van der Waals interactions energies of the residue under mutation with its surroundings are calculated in MD simulations of the complex and of the subunit. The changes of these two energies upon binding are then used in a linear regression against a training data set. In this context, we note that many other quantities, including the various components of MM-PBSA calculations [43,44] and physical descriptors such the number of interfacial salt bridges and hydrogen bonds [45] have been used for linear regression. A limitation of all these methods is the requirement of a training data set.

Particularly worth mentioning are computational redesigns which have led to increased protein–protein binding affinities [46–48] or specificity [49]. These redesign methods use physically-based energy functions. These functions involve a large number of parameters, but these parameters are pre-fixed and not adjusted for predicting binding affinities.

4. PREDICTION OF BINDING RATES

The critical role of protein–protein and protein–nucleic acid binding rates is obvious in biological processes in which speed is of the essence [50]. One such example is provided by the purple cone snail, which captures its prey with remarkable efficiency and speed through releasing a polypeptide toxin that rapidly binds to a potassium channel [51]. Compelling arguments can be made for the biological roles of rapid binding in general [52]. In particular, when several proteins compete for the same receptor or when one protein is faced with alternative

pathways, kinetic control, not thermodynamic control, dominates for much of the time. Differences in binding rate between related proteins may serve as an additional mechanism for specificity. In short, rapid binding may be as important as high affinity in the proper functioning of proteins. In designing drugs targeting protein–protein interactions, both binding affinity and binding rate may have to be taken into consideration.

4.1 Overview of protein binding rates

Experimentally observed binding rates cover a wide spectrum, from $< 10^3\ M^{-1}\,s^{-1}$ to $\sim 10^{10}\ M^{-1}\,s^{-1}$ (Figure 4.4). To gain an overview on the wide variation in binding rates, we have considered the binding of two proteins (A and B) as going through an intermediate state (A*B), in which the two proteins have near-native separations and orientations [53,54]. We refer to the intermediate state as the transient complex (its precise specification is given below; a related but more loosely defined term is encounter complex). It is of interest to note that NMR has enabled visualization of the transient complex [55]. From the transient complex, conformational rearrangement can lead to the native complex (AB). Accordingly we have the kinetic scheme

$$A + B \underset{k_{-D}}{\overset{k_D}{\rightleftharpoons}} A * B \xrightarrow{k_c} C\ . \tag{3}$$

The overall binding is

$$k_a = \frac{k_D k_c}{k_{-D} + k_c} \tag{4}$$

which is bounded by the diffusion-controlled rate, k_D, for reaching the transient complex. This limit is reached when conformational rearrangement is fast (i.e., $k_c \gg k_{-D}$), leading to

$$k_a \approx k_D. \tag{5}$$

At the other end of the spectrum, conformational rearrangement is rate-limiting (i.e., $k_c \ll k_{-D}$), and

$$k_a \approx k_c k_D / k_{-D} \equiv k_R. \tag{6}$$

Note that k_D/k_{-D} is the equilibrium constant for forming the transient complex.

In the transient complex the two protein molecules must satisfy translational/rotational constraints, which severely hinder the diffusion-controlled rate k_D. In the absence of any biasing force, theoretical estimates put the basal value, k_{D0}, in the range of 10^5 to $10^6\ M^{-1}\,s^{-1}$ [56–58]. In particular, antibody-protein binding rates are typically observed in this narrow range [59–61]. The value $10^5\ M^{-1}\,s^{-1}$ thus marks the start of the diffusion-controlled regime (Figure 4.4). A rate much lower than $10^5\ M^{-1}\,s^{-1}$ is an indication that conformational change plays a significant role in the association.

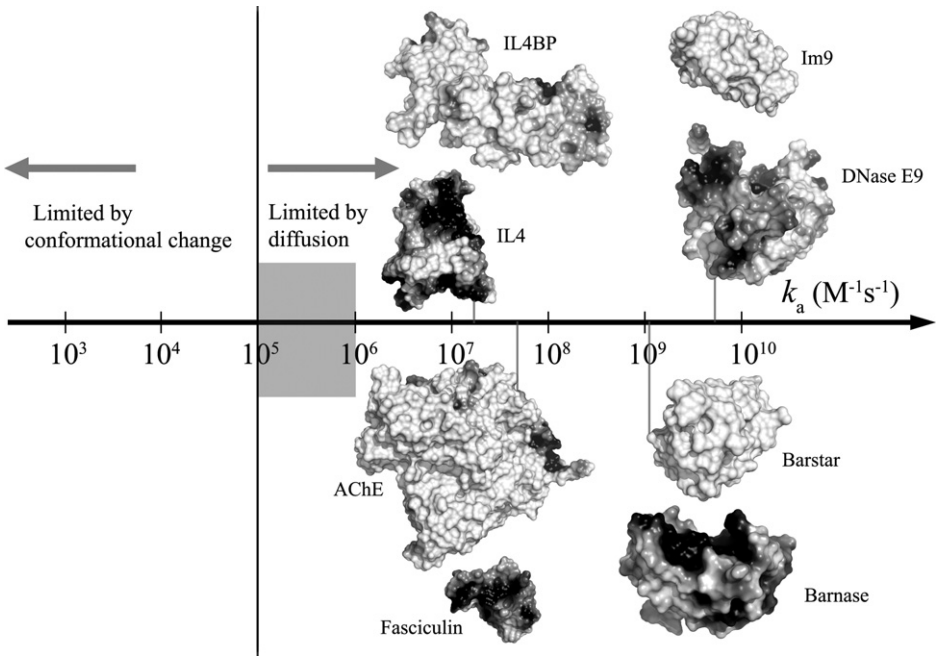

FIGURE 4.4 The spectrum of protein binding rates. The different regimes are indicated by arrows. For protein complexes in the electrostatically-enhanced regime are shown. Adapted from Alsallaq and Zhou [19].

To go beyond the basal rate k_{D0} and reach rates like 10^8 to 10^9 $M^{-1}\,s^{-1}$ as observed for many protein complexes [62–69] (Figure 4.4), intermolecular forces must be present. For a force to speed up a diffusion-controlled binding, it must be present in the diffusion process that leads to the transient complex, and thus be long-ranged. Indeed, analytical results on model systems show that, when the range of the force is reduced, the resulting rate enhancement decreases drastically [57,70,71]. For protein–protein and protein–nucleic acid binding, the dominant long-range force is provided by electrostatic interactions. Rates higher than k_{D0} require favorable electrostatic interactions, which are manifested by complementary charge distributions on the two binding partners.

4.2 Brownian dynamics simulations

Many groups have used Brownian dynamics (BD) simulations to calculate the diffusion-controlled rate k_D [56,72–84] or to generate the loosely defined encounter complex [85–87]. In rate calculations one must specify a precise set of conditions, which when satisfied signifies the formation of the native complex. Specifying this set of conditions, typically implemented as an absorbing boundary in BD simulations, is equivalent to defining the transient complex. Rather than being guided by any theoretical considerations, the location of the absorbing boundary is typically proposed in an ad hoc way, and often adjusted for best agreement with experiment. Two alternative algorithms are available for obtaining k_D from statistics accumulated on BD trajectories. In one the trajectories of a protein are started from a spherical surface around the receptor [88]. In the other, the pair of binding molecules are started in the vicinity of the absorbing boundary [89].

Electrostatic interactions are accounted for by their influence on the translational and rotational Brownian motion of the binding molecules. In principle, the electrostatic force and torque on the molecules can be calculated from solving the PB equation. However, solving the PB equation on the fly during a BD simulation is prohibitively expensive. One thus has to rely on approximations, such as treating one of the proteins as a set of test charges [72] (which leads to significant errors from neglecting the low-dielectric region of the protein interior [73]) or a more elaborate effective-charge model [90]. Unfortunately, the approximations are worst when the proteins are in close proximity, precisely where electrostatic interactions are expected to have the strongest influence on k_D.

4.3 Transient-complex theory

From BD simulations [54,73,91,92] and analytical results [57,93], it was discovered that the diffusion-controlled rate can be accurately approximated as

$$k_D = k_{D0}\, e^{-\langle W_{el}\rangle^*/k_B T} \tag{7}$$

where k_{D0} is the basal rate, i.e., the rate when electrostatic interactions are turned off, and the average $\langle\cdots\rangle^*$ is over the configurational space of the transient complex. This equation resolves one of the two main obstacles to reliable prediction of binding rates, by making it possible to rigorously treat electrostatic interactions. The effect of electrostatic interactions is captured by the Boltzmann factor

$e^{-\langle W_{el}\rangle^*/k_BT}$, which can be obtained by averaging over a relatively small number of representative configurations in the transient complex. The basal rate k_{D0} still needs to be obtained through force-free BD simulations, but these simulations are inexpensive.

The remaining obstacle to reliable prediction of protein association rates is the specification of the transient complex. The ad hoc way by which the set of conditions for complex formation—which is the equivalent of the transition complex—is specified in BD simulations is noted above. The application of Eq. (7) for predicting k_D faces a similar situation. In an early application to the binding of barnase and barstar [94], the transient-complex ensemble was specified by adjusting the ranges of translation and rotation between the two proteins to match the experimental data at high ionic strength. Similarly, Miyashita et al. [95] used experimental data for the binding of cytochrome *c*2 and bacterial reaction center to locate the transient-complex ensemble in the 6-dimensional translation-rotation configurational space.

For Eq. (7) to have predictive power, the transient-complex ensemble has to be specified without reference to experiment. A solution to this challenging problem was proposed in a recent paper [15], based on analyzing the interaction energy landscape of binding proteins. The basic idea is as follows. In a complete theory, the overall binding rate k_a should not be sensitive to where the transient complex is placed. If it is placed far away from the native complex, then k_D will be large but k_c will be small. Conversely, if it is placed very close to the native complex, then k_D will be reduced but k_c will become very large. Either way, Eq. (4) is expected to give nearly the same result for k_a. However, given the considerable difficulty and uncertainty in the calculation of k_c, it is highly desirable to use k_D as a good approximation for k_a. Then there is an optimal location for placing the transient complex [96]. If it is placed too far from the native complex, then the resulting k_D would not be a useful approximation for k_a. On the other hand, placing the transient complex too close to the native complex would mean that short-range interactions and conformational rearrangement have to be dealt with in calculating k_D. The native complex sits in a deep well in the interaction energy landscape [15]. The optimal placement for the transient-complex ensemble is at the outer boundary of the native-complex energy well [15,96].

The specific procedure implementing this basic idea was based on the following observation: inside the native-complex energy well, translation and rotation are restricted, but once outside the two proteins gain significant translational and rotational freedom [15]. Thus the outer boundary of the native-complex energy well coincides with the onset of translational and rotational freedom. This onset was located by monitoring the allowed range of a relative rotation angle between the proteins as they move out of the native-complex energy well.

This structural model for the transient-complex ensemble along with Eq. (7) constitutes the transient-complex theory for predicting protein binding rates. In this theory, both of the obstacles faced by the traditional approach of BD simulations are resolved. Electrostatic interactions can be treated rigorously, and the transient complex is specified solely based on theoretical consideration.

In Eq. (7), only the electrostatic contribution to the interaction energy of the transient complex is included. The neglect of short-ranged non-electrostatic effects from the Boltzmann factor in Eq. (7) can be understood from two considerations. First, the transient-complex configurations are typically separated by at least one layer of solvent [15], therefore short-ranged forces such as hydrophobic and van der Waals interactions are relatively weak in the diffusion process leading to the transient complex. Second, as already noted in Section 4.1, compared to long-range interactions, short-range interactions, even when present within the transient complex, contribute much less to rate enhancement (i.e., k_D/k_{D0}). Including their contribution to the interaction energy in the Boltzmann factor will significantly overestimate their effect on rate enhancement. However, short-ranged interactions are essential for determining the location and size of the transient-complex ensemble in configurational space, which in turn affect the magnitude of k_{D0}. A transient-complex ensemble that is less restricted in translation and rotation will lead to a higher k_{D0}. Variation of the restriction in translation and rotation within the transient complex with solvent conditions or among different protein complexes can be viewed as a configurational entropy effect. The basal rate k_{D0} captures this entropy effect.

It has been noted that electrostatically enhanced protein binding exhibits an interesting tell-tale sign: the binding and unbinding rate constants show disparate dependences on ionic strength [96,97]. The binding rate decreases significantly with increasing ionic strength, whereas the unbinding rate is only modestly affected by ionic strength. The structural model for the transient-complex ensemble provides a nice explanation for the disparate effects of ionic strength. As the transient complex lies at the outer boundary of the interaction energy well and hence is close to the native complex, ionic strength is expected to screen electrostatic interactions in the two types of complexes to nearly the same extent. Hence the binding affinity and the binding rate are expected to have nearly the same dependence on ionic strength and the dissociation rate would be little affected by ionic strength.

The transient-complex theory has been put to a comprehensive test against experimental data [62–64,98] for the binding rates of four protein pairs (shown in Figure 4.4) and 23 of their mutants over wide ranges of ionic strength [52]. The ionic strength dependences of the binding rates for all the four protein pairs are predicted well by the theory. Moreover, the predictions for 23 mutants at various ionic strengths agree closely with experiment. In all there are 81 data points in the latter comparison, spanning four orders of magnitude in association rate. The theory thus appears to fulfill the promise of having truly predictive power. It reveals that, among the protein pairs and their mutants studied, the basal rate k_{D0} can differ by ~20-fold, but the bulk of the variations in k_D is due to the variations in $\langle W_{el}\rangle^*$, which ranges from 0 to −6 kcal/mol (the last value translates into a 10^4-fold rate enhancement).

The above comparison against experiment was based on calculating the electrostatic interaction energy from the linearized PB equation. It has been found that, when the full PB equation was used, agreement with experiment improved, albeit modestly [19]. This underscores the point that a rigorous treatment of electrostatic interactions is essential for the accuracy of calculated k_D.

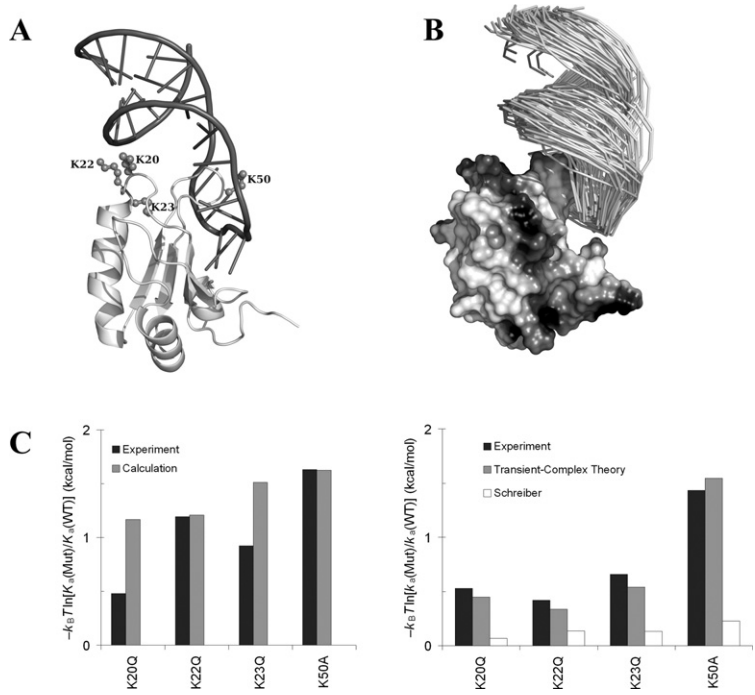

FIGURE 4.5 Binding of U1A and U1 RNA. (A) The native complex, with side chains of K20, K22, K23, and K50 of U1A shown. (B) Representative configurations in the transient complex. (C) Comparison of calculated and experimental results for the effects of mutating four lysine residues on the binding rate. Parts (A) and (B) are adapted from Qin and Zhou [71]. The left panel in (C) is taken from Qin and Zhou [18], and the right panel in (C) is taken from Qin and Zhou [71], but with the additional result label Schreiber calculated according to Selzer et al. [103].

For the binding between a protein and an RNA, the difference between the full PB equation and the linearized version is no longer modest because of the large charge density on the nucleic acid. Then use of the full PB equation becomes a necessity. The transient-complex theory has made it possible to realistically model protein–RNA binding rates for the first time [71]. In this work the binding of the spliceosomal protein U1A and its target on the U1 small nuclear RNA (Figure 4.5A) was studied. The binding and unbinding rates of this and other protein–RNA systems exhibit the disparate dependences on salt familiar to proteins [99–102], indicating that the structural model for the transient complex developed for protein–protein binding is applicable to protein–RNA binding. Representative configurations in the transient complex of the U1 system are shown in Figure 4.5B. The binding rates of the wild-type system and eight of its mutants predicted by the transient-complex theory are in close agreement with experiment [99, 101] (Figure 4.5C).

Comparison of predicted and experimental binding rates also help settle the debate between MS and vdW as the choice for the dielectric boundary in cal-

culating the electrostatic interaction energy. The rate predictions summarized above have all been obtained by using the vdW protocol in calculating $\langle W_{el}\rangle^*$. With the MS protocol, the sign of $\langle W_{el}\rangle^*$ switches to positive (similar to what is seen on native complexes [16,17]) and now rate retardation is predicted [19]! For example, for the barnase–barstar pair, when the ionic strength is varied from 13 mM to 2000 mM, $\langle W_{el}\rangle^*$ calculated with the vdW protocol varied from −3.30 to −0.82 kcal/mol. Correspondingly, $\langle W_{el}\rangle^*$ calculated with MS protocol varied from 2.50 to 5.13 kcal/mol. For the latter results to be consistent with experiment, a basal rate in the order of 10^{10}–10^{11} $M^{-1}\,s^{-1}$ would be required, which clearly seems unphysical.

While the transient-complex theory is not appropriate for binding processes that are limited by large-scale conformational rearrangements, it can accommodate local conformational fluctuations. In particular, MD simulations have shown that charged side chains that eventually form cross-interface salt bridges in the native complex can form intramolecular salt bridges prior to reaching the transient complex [85]. More generally, local conformation populations in the transient complex will be different from those in the native complex. While applications of the transient-complex theory have so far assumed native conformations in the transient complex, more accurate calculations may require conformational sampling specifically within the transient complex.

4.4 Further approximation and rate enhancement by design

Based on Eq. (7), Schreiber and co-workers have made a further simplification [103–105]. Instead of using the transient-complex ensemble, they calculated $\langle W_{el}\rangle^*$ by applying an empirical function directly to the native complex. The empirical function effectively reduces the interaction energy calculated on the native complex to make it appropriate for the transient complex, and is parameterized on experimental data. Despite the approximation, the simplified approach has allowed them to design charge mutations that lead to as much as 250-fold increase in binding rate.

As an estimate for $\langle W_{el}\rangle^*$, a weaken version of the electrostatic interaction energy of the native complex seems capable of capturing general trends, but it has limitation in accounting for specific contributions of individual residues. This limitation is illustrated by the effects of mutating four lysine residues on the binding rate of U1A with U1 RNA. In the native complex (Figure 4.5A), K50 protrudes deeply into the RNA loop and lies above it, while K20, K22, and K23 lie below the loop. The four lysines have comparable separations from the RNA and their neutralizations reduce the binding free energy to similar extents (Figure 4.5C, left panel). The approach of Schreiber and co-workers would predict that the neutralizations reduce the binding rate to similar extents (Figure 4.5C, right panel). In the transient complex (Figure 4.5B), the RNA moves away from U1A, consequently K20, K22, and K23 are placed further away from the RNA. In contrast, because of its protruded position, the separation of K50 from RNA is not significantly reduced. As a result, in the transient complex the electrostatic contributions of K20, K22, and K23 are significantly reduced but that of K50 is nearly unchanged when

compared to the native complex. This contrast between K20, K22, and K23 on the one hand and K50 on the other is supported by experimental results [99,101] (Figure 4.5C, right panel).

5. DYNAMICS WITHIN NATIVE COMPLEXES AND DURING COMPLEX FORMATION

The foregoing discussions make it clear that protein dynamics presents challenges for building structural models of protein complexes, makes important contributions to binding affinity, and is an integral part of the binding process. Recent experiments have presented direct evidence for the contribution of protein dynamics to binding affinity [106,107]. Changes in conformation and in dynamics upon complex formation have been studied by NMR [108–110] and by MD simulations [111]. Conformational rearrangements leading to native complexes have also been revealed by MD simulations [85,112], which as noted above may be required for more accurate calculations of binding rates within the transient-complex theory. These studies have laid the groundwork toward a comprehensive understanding of the roles of dynamics in protein–protein and protein–nucleic acid interactions.

6. SUMMARY POINTS

1. Structures of protein complexes are the basis for understanding protein interactions. Many of these structures will have to be built by docking. CAPRI provides a forum for critical assessment of docking methods. Methods making use of experimental or predicted interface information appear promising.
2. Predicting absolute binding free energy is still formidable, but there is significant progress in predicting relative binding free energy. Contributions of electrostatic interactions are sensitive to model details, in particular the choice of the boundary between the protein low dielectric and solvent high dielectric. Experimental data such as mutational effects on binding affinity are useful for selecting calculation models.
3. The wide variation of binding rates among protein complexes can be understood by considering rate-limiting conformational changes in one extreme and electrostatic rate enhancement in the opposite extreme. Current theory has shown predictive power for binding rates in the diffusion-controlled regime (i.e., those above $\sim 10^5\ M^{-1}\ s^{-1}$).
4. Experiments and MD simulations are contributing toward a comprehensive understanding of the roles of dynamics in the various aspects of protein interactions.

ACKNOWLEDGMENTS

This work was supported in part by Grant GM058187 from the National Institutes of Health.

REFERENCES

1. Aloy, P., Bottcher, B., Ceulemans, H., Leutwein, C., Mellwig, C., Fischer, S., Gavin, A.C., Bork, P., Superti-Furga, G., Serrano, L., Russell, R.B. Structure-based assembly of protein complexes in yeast. Science 2004, 303, 2026–9.
2. Contreras-Moreira, B., Branger, P.A., Collado-Vides, J. TFmodeller: Comparative modelling of protein-DNA complexes. Bioinformatics 2007, 23, 1694–6.
3. Yi, M., Tjong, H., Zhou, H.X. Spontaneous conformational change and toxin binding in $\alpha 7$ nicotinic acetylcholine receptor: Insight into channel activation and inhibition. Proc. Natl. Acad. Sci. USA 2008, 105, 8280–5.
4. Tang, C., Clore, G.M. A simple and reliable approach to docking protein–protein complexes from very sparse NOE-derived intermolecular distance restraints. J. Biomol. NMR 2006, 36, 37–44.
5. Qin, S., Zhou, H.X. A holistic approach to protein docking. Proteins 2007, 69, 743–9.
6. Bhatnagar, J., Freed, J.H., Crane, B.R. Rigid body refinement of protein complexes with long-range distance restraints from pulsed dipolar ESR. Methods Enzymol. 2007, 423, 117–33.
7. Motiejunas, D., Gabdoulline, R., Wang, T., Feldman-Salit, A., Johann, T., Winn, P.J., Wade, R.C. Protein–protein docking by simulating the process of association subject to biochemical constraints. Proteins 2008, 71, 1955–69.
8. Zhou, H.X., Qin, S. Interaction-site prediction for protein complexes: A critical assessment. Bioinformatics 2007, 23, 2203–9.
9. Korkin, D., Davis, F.P., Alber, F., Luong, T., Shen, M.Y., Lucic, V., Kennedy, B.M., Sali, A. Structural modeling of protein interactions by analogy: Application to PSD-95. PLoS Comput. Biol. 2006, 2, e153.
10. Gunther, S., May, P., Hoppe, A., Frommel, C., Preissner, R. Docking without docking: ISEARCH—Prediction of interactions using known interfaces. Proteins 2007, 69, 839–44.
11. Yang, C.-Y., Wang, S.M. Recent advances in design of small-molecule ligands to target protein–protein interactions. In: Annual Reports in Computational Chemistry, vol. 2. 2006, pp. 197–219.
12. Huang, P.S., Love, J.J., Mayo, S.L. A de novo designed protein–protein interface. Protein Sci. 2007, 16, 2770–4.
13. Liu, S., Liu, S., Zhu, X., Liang, H., Cao, A., Chang, Z., Lai, L. Nonnatural protein–protein interaction-pair design by key residues grafting. Proc. Natl. Acad. Sci. USA 2007, 104, 5330–5.
14. Gilson, M.K., Zhou, H.X. Calculation of protein–ligand binding affinities. Annu. Rev. Biophys. Biomol. Struct. 2007, 36, 21–42.
15. Alsallaq, R., Zhou, H.X. Energy landscape and transition state of protein–protein association. Biophys. J. 2007, 92, 1486–502.
16. Vijayakumar, M., Dong, F., Zhou, H.X. Comparison of calculation and experiment implicates significant electrostatic contributions to the binding stability of barnase and barstar. Biophys. J. 2003, 85, 49–60.
17. Dong, F., Zhou, H.X. Electrostatic contribution to the binding stability of protein–protein complexes. Proteins 2006, 65, 87–102.
18. Qin, S., Zhou, H.X. Do electrostatic interactions destabilize protein-nucleic acid binding? Biopolymers 2007, 86, 112–8.
19. Alsallaq, R., Zhou, H.X. Electrostatic rate enhancement and transient complex of protein–protein association. Proteins 2008, 71, 320–35.
20. Swanson, J.M.J., Mongan, J., McCammon, J.A. Limitations of atom-centered dielectric functions in implicit solvation models. J. Phys. Chem. B 2005, 109, 14769–72.
21. Tan, C., Yang, L., Luo, R. How well does Poisson–Boltzmann implicit solvent agree with explicit solvent? A quantitative analysis. J. Phys. Chem. B 2006, 110, 18680–7.
22. Swanson, J.M.J., Wagoner, J.A., Baker, N.A., McCammon, J.A. Optimizing the Poisson dielectric boundary with explicit solvent forces and energies: Lessons learned with atom-centered dielectric functions. J. Chem. Theo. Comp. 2007, 3, 170–83.
23. Tjong, H., Zhou, H.X. On the dielectric boundary in Poisson–Boltzmann calculations. J. Chem. Theo. Comp. 2008, 4, 507–14.
24. del Alamo, M., Mateu, M.G. Electrostatic repulsion, compensatory mutations, and long-range non-additive effects at the dimerization interface of the HIV capsid protein. J. Mol. Biol. 2005, 345, 893–906.

25. Pal, G., Kouadio, J.L., Artis, D.R., Kossiakoff, A.A., Sidhu, S.S. Comprehensive and quantitative mapping of energy landscapes for protein–protein interactions by rapid combinatorial scanning. J. Biol. Chem. 2006, 281, 22378–85.
26. Ernst, J.A., Clubb, R.T., Zhou, H.-X., Gronenborn, A.M., Clore, G.M. Demonstration of positionally disordered water within a protein hydrophobic cavity by NMR. Science 1995, 267, 1813–7.
27. Damjanovic, A., Garcia-Moreno, B., Lattman, E.E., Garcia, A.E. Molecular dynamics study of water penetration in staphylococcal nuclease. Proteins 2005, 60, 433–49.
28. Still, A., Tempczyk, W.C., Hawley, R.C., Hendrikson, R. Semianalytical treatment of solvation for molecular mechanics and dynamics. J. Am. Chem. Soc. 1990, 112, 6127–9.
29. Lee, M.S., Feig, M., Salsbury Jr., F.R., Brooks III, C.L. New analytic approximation to the standard molecular volume definition and its application to generalized Born calculations. J. Comput. Chem. 2003, 24, 1348–56.
30. Onufriev, A., Bashford, D., Case, D.A. Exploring protein native states and large-scale conformational changes with a modified generalized Born model. Proteins 2004, 55, 383–94.
31. Tjong, H., Zhou, H.-X. GBr^6: A parameterization-free, accurate, analytical generalized Born method. J. Phys. Chem. B 2007, 111, 3055–61.
32. Guallar, V., Borrelli, K.W. A binding mechanism in protein–nucleotide interactions: Implication for U1A RNA binding. Proc. Natl. Acad. Sci. USA 2005, 102, 3954–9.
33. Ababou, A., van der Vaart, A., Gogonea, V., Merz Jr., K.M. Interaction energy decomposition in protein–protein association: A quantum mechanical study of barnase–barstar complex. Biophys. Chem. 2007, 125, 221–36.
34. Massova, I., Kollman, P.A. Computational alanine scanning to probe protein–protein interactions: A novel approach to evaluate binding free energies. J. Am. Chem. Soc. 1999, 121, 8133–43.
35. Reyes, C.M., Kollman, P.A. Structure and thermodynamics of RNA–protein binding: Using molecular dynamics and free energy analyses to calculate the free energies of binding and conformational change. J. Mol. Biol. 2000, 297, 1145–56.
36. Gohlke, H., Kiel, C., Case, D.A. Insights into protein–protein binding by binding free energy calculation and free energy decomposition for the Ras–Raf and Ras–RalGDS complexes. J. Mol. Biol. 2003, 330, 891–913.
37. Luo, C., Xu, L., Zheng, S., Luo, X., Shen, J., Jiang, H., Liu, X., Zhou, M. Computational analysis of molecular basis of 1:1 interactions of NRG-1beta wild-type and variants with ErbB3 and ErbB4. Proteins 2005, 59, 742–56.
38. Basdevant, N., Weinstein, H., Ceruso, M. Thermodynamic basis for promiscuity and selectivity in protein–protein interactions: PDZ domains, a case study. J. Am. Chem. Soc. 2006, 128, 12766–77.
39. Hou, T., Chen, K., McLaughlin, W.A., Lu, B., Wang, W. Computational analysis and prediction of the binding motif and protein interacting partners of the Abl SH3 domain. PLoS Comput. Biol. 2006, 2, e1.
40. Moreira, I.S., Fernandes, P.A., Ramos, M.J. Computational alanine scanning mutagenesis—An improved methodological approach. J. Comput. Chem. 2007, 28, 644–54.
41. Zoete, V., Michielin, O. Comparison between computational alanine scanning and per-residue binding free energy decomposition for protein–protein association using MM-GBSA: Application to the TCR-p-MHC complex. Proteins 2007, 67, 1026–47.
42. Almlof, M., Aqvist, J., Smalas, A.O., Brandsdal, B.O. Probing the effect of point mutations at protein–protein interfaces with free energy calculations. Biophys. J. 2006, 90, 433–42.
43. Zhou, Z., Bates, M., Madura, J.D. Structure modeling, ligand binding, and binding affinity calculation (LR-MM-PBSA) of human heparanase for inhibition and drug design. Proteins 2006, 65, 580–92.
44. Kormos, B.L., Benitex, Y., Baranger, A.M., Beveridge, D.L. Affinity and specificity of protein U1A-RNA complex formation based on an additive component free energy model. J. Mol. Biol. 2007, 371, 1405–19.
45. Audie, J., Scarlata, S. A novel empirical free energy function that explains and predicts protein–protein binding affinities. Biophys. Chem. 2007, 129, 198–211.
46. Clark, L.A., Boriack-Sjodin, P.A., Eldredge, J., Fitch, C., Friedman, B., Hanf, K.J., Jarpe, M., Liparoto, S.F., Li, Y., Lugovskoy, A., Miller, S., Rushe, M., Sherman, W., Simon, K., Van Vlijmen, H. Affinity enhancement of an in vivo matured therapeutic antibody using structure-based computational design. Protein Sci. 2006, 15, 949–60.

47. Song, G., Lazar, G.A., Kortemme, T., Shimaoka, M., Desjarlais, J.R., Baker, D., Springer, T.A. Rational design of intercellular adhesion molecule-1 (ICAM-1) variants for antagonizing integrin lymphocyte function-associated antigen-1-dependent adhesion. J. Biol. Chem. 2006, 281, 5042–9.
48. Sammond, D.W., Eletr, Z.M., Purbeck, C., Kimple, R.J., Siderovski, D.P., Kuhlman, B. Structure-based protocol for identifying mutations that enhance protein–protein binding affinities. J. Mol. Biol. 2007, 371, 1392–404.
49. Joachimiak, L.A., Kortemme, T., Stoddard, B.L., Baker, D. Computational design of a new hydrogen bond network and at least a 300-fold specificity switch at a protein–protein interface. J. Mol. Biol. 2006, 361, 195–208.
50. Zhou, H.-X. How do biomolecular systems speed up and regulate rates of processes? Phys. Biol. 2005, 2, R1–25.
51. Terlau, H., Shon, K.-J., Grilley, M., Stocker, M., Stuhmer, W., Baldomero, O.M. Strategy for rapid immobilization of prey by a fish-hunting marine snail. Nature 1996, 381, 148–51.
52. Alsallaq, R., Zhou, H.-X. Prediction of protein–protein association rates from a transition-state theory. Structure 2007, 15, 215–24.
53. Alsallaq, R., Zhou, H.-X. Electrostatic rate enhancement and transient complex of protein–protein association. Proteins 2007, 71, 320–35.
54. Zhou, H.-X., Wong, K.Y., Vijayakumar, M. Design of fast enzymes by optimizing interaction potential in active site. Proc. Natl. Acad. Sci. USA 1997, 94, 12372–7.
55. Tang, C., Iwahara, J., Clore, G.M. Visualization of transient encounter complexes in protein–protein association. Nature 2006, 444, 383–6.
56. Northrup, S.H., Erickson, H.P. Kinetics of protein–protein association explained by Brownian dynamics computer simulation. Proc. Natl. Acad. Sci. USA 1992, 89, 3338–42.
57. Zhou, H.-X. Enhancement of protein–protein association rate by interaction potential: Accuracy of prediction based on local Boltzmann factor. Biophys. J. 1997, 73, 2441–5.
58. Schlosshauer, M., Baker, D. Realistic protein–protein association rates from a simple diffusional model neglecting long-range interactions, free energy barriers, and landscape ruggedness. Protein Sci. 2004, 13, 1660–9.
59. Foote, J., Eisen, H.N. Kinetic and affinity limits on antibodies produced during immune responses. Proc. Natl. Acad. Sci. USA 1995, 92, 1254–6.
60. Hoffman, T.L., LaBranche, C.C., Zhang, W., Canziani, G., Robinson, J., Chaiken, I., Hoxie, J.A., Doms, R.W. Stable exposure of the coreceptor-binding site in a CD4-independent HIV-1 envelope protein. Proc. Natl. Acad. Sci. USA 1999, 96, 6359–64.
61. Wassaf, D., Kuang, G., Kopacz, K., Wu, Q.L., Nguyen, Q., Toews, M., Cosic, J., Jacques, J., Wiltshire, S., Lambert, J., Pazmany, C.C., Hogan, S., Ladner, C.R., Nixon, A.E., Sexton, D.J. High-throughput affinity ranking of antibodies using surface plasmon resonance microarrays. Anal. Biochem. 2006, 351, 241–53.
62. Wallis, R., Moore, G.K., James, R., Kleanthous, C. Protein–protein interactions in colicin E9 DNase-immunity protein complexes. 1. Diffusion-controlled association and femtomolar binding for the cognate complex. Biochemistry 1995, 34, 13743–50.
63. Schreiber, G., Fersht, A.R. Rapid, electrostatically assisted association of proteins. Nat. Struct. Biol. 1996, 3, 427–31.
64. Radic, Z., Kirchhoff, P.D., Quinn, D.M., McCammon, J.A., Taylor, P. Electrostatic influence on the kinetics of ligand binding to acetylcholinesterase. J. Biol. Chem. 1997, 272, 23265–77.
65. Shapiro, R., Ruiz-Gutierrez, M., Chen, C.-Z. Analysis of the interactions of human ribonuclease inhibitor with angiogenin and ribonuclease A by mutagenesis: Importance of inhibitor residues inside versus outside the C-terminal "hot spot". J. Mol. Biol. 2000, 302, 497–519.
66. Darling, R.J., Kuchibhotla, U., Glaesner, W., Micanovic, R., Witcher, D.R., Beals, J.M. Glycosylation of erythropoietin affects receptor binding kinetics: Role of electrostatic interactions. Biochemistry 2002, 41, 14524–31.
67. Uter, N.T., Gruic-Sovulj, I., Perona, J.J. Amino acid-dependent transfer RNA affinity in a class I aminoacyl-tRNA synthetase. J. Biol. Chem. 2005, 280, 23966–77.
68. Korennykh, A.V., Piccirilli, J.A., Correll, C.C. The electrostatic character of the ribosomal surface enables extraordinarily rapid target location by ribotoxins. Nat. Struct. Mol. Biol. 2006, 13, 436–43.
69. Johnson, R.J., McCoy, J.G., Bingman, C.A., Phillips Jr., G.N., Raines, R.T. Inhibition of human pancreatic ribonuclease by the human ribonuclease inhibitor protein. J. Mol. Biol. 2007, 368, 434–49.

70. Zhou, H.-X., Szabo, A. Enhancement of association rates by nonspecific binding to DNA and cell membranes. Phys. Rev. Lett. 2004, 93, 17810–1.
71. Qin, S., Zhou, H.X. Prediction of salt and mutational effects on the association rate of U1A protein and U1 small nuclear RNA stem/loop II. J. Phys. Chem. B 2008, 112, 5955–60.
72. Northrup, S.H., Reynolds, J.C.L., Miller, C.M., Forrest, K.J., Boles, J.O. Diffusion-controlled association rate of cytochrome c and cytochrome c peroxidase in a simple electrostatic model. J. Am. Chem. Soc. 1986, 108, 8162–70.
73. Zhou, H.-X. Brownian dynamics study of the influences of electrostatic interaction and diffusion on protein–protein association kinetics. Biophys. J. 1993, 64, 1711–26.
74. Gabdoulline, R.R., Wade, R.C. Simulation of the diffusional association of barnase and barstar. Biophys. J. 1997, 72, 1917–29.
75. Elcock, A.H., Gabdoulline, R.R., Wade, R.C., McCammon, J.A. Computer simulation of protein–protein association kinetics: Acetylcholinesterase-fasciculin. J. Mol. Biol. 1999, 291, 149–62.
76. Altobelli, G., Subramaniam, S. Kinetics of association of anti-lysozyme monoclonal antibody D44.1 and hen-egg lysozyme. Biophys. J. 2000, 79, 2954–65.
77. Fogolari, F., Ugolini, R., Molinari, H., Viglino, P., Esposito, G. Simulation of electrostatic effects in Fab-antigen complex formation. Eur. J. Biochem. 2000, 267, 4861–9.
78. Gabdoulline, R.R., Wade, R.C. Protein–protein association: Investigation of factors influencing association rates by Brownian dynamics simulations. J. Mol. Biol. 2001, 306, 1139–55.
79. De Rienzo, F., Gabdoulline, R.R., Menziani, M.C., De Benedetti, P.G., Wade, R.C. Electrostatic analysis and Brownian dynamics simulation of the association of plastocyanin and cytochrome f. Biophys. J. 2001, 81, 3090–104.
80. Zou, G., Skeel, R.D. Robust biased Brownian dynamics for rate constant calculation. Biophys. J. 2003, 85, 2147–57.
81. Ermakova, E. Lysozyme dimerization: Brownian dynamics simulation. J. Mol. Model 2005, 12, 34–41.
82. Lin, J., Beratan, D.N. Simulation of electron transfer between cytochrome c2 and the bacterial photosynthetic reaction center: Brownian dynamics analysis of the native proteins and double mutants. J. Phys. Chem. B 2005, 109, 7529–34.
83. Gross, E.L., Rosenberg, I. A Brownian dynamics study of the interaction of phormidium cytochrome f with various cyanobacterial plastocyanins. Biophys. J. 2006, 90, 366–80.
84. Blachut-Okrasinska, E., Antosiewicz, J.M. Brownian dynamics simulations of binding mRNA cap analogues to eIF4E protein. J. Phys. Chem. B 2007, 111, 13107–15.
85. Huang, X., Dong, F., Zhou, H.X. Electrostatic recognition and induced fit in the kappa-PVIIA toxin binding to Shaker potassium channel. J. Am. Chem. Soc. 2005, 127, 6836–49.
86. Spaar, A., Dammer, C., Gabdoulline, R.R., Wade, R.C., Helms, V. Diffusional encounter of barnase and barstar. Biophys. J. 2006, 90, 1913–24.
87. Forlemu, N.Y., Waingeh, V.F., Ouporov, I.V., Lowe, S.L., Thomasson, K.A. Theoretical study of interactions between muscle aldolase and F-actin: Insight into different species. Biopolymers 2007, 85, 60–71.
88. Northrup, S.H., Allison, S.A., McCammon, J.A. Brownian dynamics simulation of diffusion-influenced bimolecular reactions. J. Chem. Phys. 1984, 80, 1517–24.
89. Zhou, H.-X. Kinetics of diffusion-influenced reactions studied by Brownian dynamics. J. Phys. Chem. 1990, 94, 8794–800.
90. Gabdoulline, R.R., Wade, R.C. Effective charges for macromolecules in solvent. J. Phys. Chem. 1996, 100, 3868–78.
91. Zhou, H.-X., Briggs, J.M., McCammon, J.A. A 240-fold electrostatic rate-enhancement for acetylcholinesterase-substrate binding can be predicted by the potential within the active site. J. Am. Chem. Soc. 1996, 118, 13069–70.
92. Zhou, H.-X., Briggs, J.M., Tara, S., McCammon, J.A. Correlation between rate of enzyme-substrate diffusional encounter and average Boltzmann factor around active site. Biopolymers 1998, 45, 355–60.
93. Zhou, H.-X. Effect of interaction potentials in diffusion-influenced reactions with small reactive regions. J. Chem. Phys. 1996, 105, 7235–7.

94. Vijayakumar, M., Wong, K.Y., Schreiber, G., Fersht, A.R., Szabo, A., Zhou, H.-X. Electrostatic enhancement of diffusion-controlled protein–protein association: Comparison of theory and experiment on barnase and barstar. J. Mol. Biol. 1998, 278, 1015–24.
95. Miyashita, O., Onuchic, J.N., Okamura, M.Y. Transition state and encounter complex for fast association of cytochrome c2 with bacterial reaction center. Proc. Natl. Acad. Sci. USA 2004, 101, 16174–9.
96. Zhou, H.-X. Disparate ionic-strength dependencies of on and off rates in protein–protein association. Biopolymers 2001, 59, 427–33.
97. Zhou, H.-X. Association and dissociation kinetics of colicin E3 and immunity protein 3: Convergence of theory and experiment. Protein Sci. 2003, 12, 2379–82.
98. Shen, B.J., Hage, T., Sebald, W. Global and local determinants for the kinetics of interleukin-4/interleukin-4 receptor alpha chain interaction. A biosensor study employing recombinant interleukin-4-binding protein. Eur. J. Biochem. 1996, 40, 252–61.
99. Katsamba, P.S., Myszka, D.G., Laird-Offringa, I.A. Two functionally distinct steps mediate high affinity binding of U1A protein to U1 hairpin II RNA. J. Biol. Chem. 2001, 276, 21476–81.
100. Milev, S., Bosshard, H.R., Jelesarov, I. Enthalpic and entropic effects of salt and polyol osmolytes on site-specific protein–DNA association: The integrase Tn916-DNA complex. Biochemistry 2005, 44, 285–93.
101. Law, M.J., Linde, M.E., Chambers, E.J., Oubridge, C., Katsamba, P.S., Nilsson, L., Haworth, I.S., Laird-Offringa, I.A. The role of positively charged amino acids and electrostatic interactions in the complex of U1A protein and U1 hairpin II RNA. Nucl. Acids Res. 2006, 34, 275–85.
102. Auweter, S.D., Fasan, R., Reymond, L., Underwood, J.G., Black, D.L., Pitsch, S., Allain, F.H. Molecular basis of RNA recognition by the human alternative splicing factor Fox-1. EMBO J. 2006, 25, 163–73.
103. Selzer, T., Albeck, S., Schreiber, G. Rational design of faster associating and tighter binding protein complexes. Nat. Struct. Biol. 2000, 7, 537–41.
104. Kiel, C., Selzer, T., Shaul, Y., Schreiber, G., Herrmann, C. Electrostatically optimized Ras-binding Ral guanine dissociation stimulator mutants increase the rate of association by stabilizing the encounter complex. Proc. Natl. Acad. Sci. USA 2004, 101, 9223–8.
105. Shaul, Y., Schreiber, G. Exploring the charge space of protein–protein association: A proteomic study. Proteins 2005, 60, 341–52.
106. Horn, J.R., Kraybill, B., Petro, E.J., Coales, S.J., Morrow, J.A., Hamuro, Y., Kossiakoff, A.A. The role of protein dynamics in increasing binding affinity for an engineered protein–protein interaction established by H/D exchange mass spectrometry. Biochemistry 2006, 45, 8488–98.
107. Frederick, K.K., Marlow, M.S., Valentine, K.G., Wand, A.J. Conformational entropy in molecular recognition by proteins. Nature 2007, 448, 325–9.
108. Shajani, Z., Drobny, G., Varani, G. Binding of U1A protein changes RNA dynamics as observed by 13C NMR relaxation studies. Biochemistry 2007, 46, 5875–83.
109. Lee, D., Walsh, J.D., Yu, P., Markus, M.A., Choli-Papadopoulou, T., Schwieters, C.D., Krueger, S., Draper, D.E., Wang, Y.X. The structure of free L11 and functional dynamics of L11 in free, L11-rRNA(58 nt) binary and L11-rRNA(58 nt)-thiostrepton ternary complexes. J. Mol. Biol. 2007, 367, 1007–22.
110. Jonker, H.R., Ilin, S., Grimm, S.K., Wohnert, J., Schwalbe, H. L11 domain rearrangement upon binding to RNA and thiostrepton studied by NMR spectroscopy. Nucl. Acids Res. 2007, 35, 441–54.
111. Grunberg, R., Nilges, M., Leckner, J. Flexibility and conformational entropy in protein–protein binding. Structure 2006, 14, 683–93.
112. Bui, J.M., Radic, Z., Taylor, P., McCammon, J.A. Conformational transitions in protein–protein association: Binding of fasciculin-2 to acetylcholinesterase. Biophys. J. 2006, 90, 3280–7.